



# UVIT Open Cluster Study. I. Detection of a White Dwarf Companion to a Blue Straggler in M67: Evidence of Formation through Mass Transfer

N. Sindhu<sup>1,2</sup> , Annapurni Subramaniam<sup>2</sup>, Vikrant V. Jadhav<sup>2,3</sup> , Sourav Chatterjee<sup>4</sup> , Aaron M. Geller<sup>5,6</sup> , Christian Knigge<sup>7</sup>, Nathan Leigh<sup>8,9</sup>, Thomas H. Puzia<sup>10</sup> , Michael Shara<sup>9</sup> , and Mirko Simunovic<sup>11,12</sup>

<sup>1</sup> Department of Physics, School of Advanced Science, VIT, Vellore-632014, India; [sindhu.n@iiap.res.in](mailto:sindhu.n@iiap.res.in)

<sup>2</sup> Indian Institute of Astrophysics, Koramangala II Block, Bangalore-560034, India

<sup>3</sup> Joint Astronomy Program and Physics Department, Indian Institute of Science, Bangalore-560012, India

<sup>4</sup> DAA, TIFR, Homi Bhabha Road, Navy Nagar, Colaba, Mumbai 400005, India

<sup>5</sup> Center for Interdisciplinary Exploration and Research in Astrophysics (CIERA) and Department of Physics & Astronomy, Northwestern University, 2145 Sheridan Road, Evanston, IL 60201, USA

<sup>6</sup> Adler Planetarium, Dept. of Astronomy, 1300 S. Lake Shore Drive, Chicago, IL 60605, USA

<sup>7</sup> School of Physics and Astronomy, University of Southampton, Highfield, Southampton SO17 1BJ, UK

<sup>8</sup> Departamento de Astronomía, Facultad de Ciencias Físicas y Matemáticas, Universidad de Concepción, Concepción, Chile

<sup>9</sup> Department of Astrophysics, American Museum of Natural History, New York, NY 10024, USA

<sup>10</sup> Institute of Astrophysics, Pontificia Universidad Católica de Chile, Av. Vicuña Mackenna 4860, 7820436 Macul, Santiago, Chile

<sup>11</sup> Gemini Observatory, 670 N Aohoku Pl, Hilo, HI 96720, USA

<sup>12</sup> Subaru Telescope, 650 N Aohoku Pl, Hilo, HI 96720, USA

Received 2019 May 23; revised 2019 July 4; accepted 2019 July 9; published 2019 August 30

## Abstract

The old open cluster M67, populated with blue straggler stars (BSSs), is a well-known test bed to study the BSS formation pathways. Here, we report the first direct detection of a white dwarf (WD) companion to a BSS in M67, using far-UV images from the Ultra-Violet Imaging telescope on *ASTROSAT*. Near-simultaneous observations in three far-UV bands combined with *Galaxy Evolution Explorer*, *International Ultraviolet Explorer*, and ground- and space-based photometric data covering a 0.14–11.5  $\mu\text{m}$  range for WOCs1007 were found to require a binary fit to its spectral energy distribution (SED), consisting of a BSS and a hot companion. On the other hand, a single spectral fit was found to be satisfactory for the SEDs of two other BSSs, WOCs1006 and WOCs2011, with the latter showing a deficient far-UV flux. The hot companion of WOCs1007 is found to have a  $T_{\text{eff}} \sim 13,250\text{--}13,750$  K and a radius of  $0.09 \pm 0.01 R_{\odot}$ . A comparison with WD models suggests it to be a low-mass WD ( $\sim 0.18 M_{\odot}$ ), in agreement with the kinematic mass from the literature. As a low-mass WD ( $< 0.4 M_{\odot}$ ) necessitates formation through mass transfer in close binaries, WOCs1007 with a known period of 4.2 days along with its fast rotation, is likely to be formed by a case A or case B binary evolution.

**Key words:** open clusters and associations: individual (M67) – stars: individual (blue stragglers, white dwarfs) – ultraviolet: stars

## 1. Introduction

In a star cluster, blue straggler stars (BSSs) are found to be brighter and bluer than stars that are close to the end of their main-sequence (MS) lifetimes, suggesting that these stars have continued to stay on the MS, defying further evolution. BSSs are believed to have gained mass resulting in a rejuvenation, though the process is not well understood. The dominant BSS formation mechanisms operating in both globular and open clusters are likely to be in some way dependent on binary stars (Knigge et al. 2009; Mathieu & Geller 2009; Leigh & Sills 2011). Three processes are suggested in the literature: (1) stellar collisions in dynamical encounters between single, binary, and triple systems (Hills & Day 1976; Geller et al. 2013); (2) transfer of material through Roche-Lobe from a close companion in a binary (McCrea 1964; Tian et al. 2006); and (3) a triple system where the doublet becomes a close binary, and merges to form a massive star (Perets & Fabrycky 2009; Naoz & Fabrycky 2014). The formation pathway by mass transfer (MT) in a binary produces a BSS with a initially hot companion, such as a white dwarf (WD). The direct observational evidence was obtained by Gosnell et al. (2015), by detecting WD companions to seven BSSs in the old open cluster, NGC 188, and by Subramaniam et al. (2016a) by detecting a post-asymptotic giant branch/horizontal branch companion to a BSS in the same cluster. In the

case of globular clusters, Knigge et al. (2008) discovered the first BSS+WD binary in the central region of 47 Tuc and recently, Sahu et al. (2019) detected a BSS+WD system in the low-density outer region of the globular cluster NGC 5466.

M67 is very rich in BSSs, where 14 are confirmed as bona fide members by Geller et al. (2015). There have been several attempts previously to detect hot companions to these BSSs, particularly from spectroscopic study using the *International Ultraviolet Explorer* (*IUE*) and UV photometry from the *Ultraviolet Imaging Telescope* (*UIT*). The seminal study by Landsman et al. (1998) used *UIT* images to detect 11 BSSs in M67. As there is a 0.5 mag uncertainty in the predicted *UIT* flux and 0.14 mag uncertainty in the measured *UIT* flux, they found strong evidence for a UV excess only in two BSSs (S975 (WOCs<sup>13</sup> 3010) and S1082 (WOCs2009, a triple system)). In particular, the absence of detection of a hot companion to WOCs1007 was surprising as this is a spectroscopic binary with a 4.2 day period and suspected to be currently undergoing MT (Milone & Latham 1992). The estimated companion mass of WOCs1007 was found to be  $0.19 M_{\odot}$  ( $M_2$  *sini*) by Milone & Latham (1992), and was suggested as a BSS+WD by Shetrone & Sandquist (2000). It should be noted that low-mass WDs, with

<sup>13</sup> WIYN open cluster study.

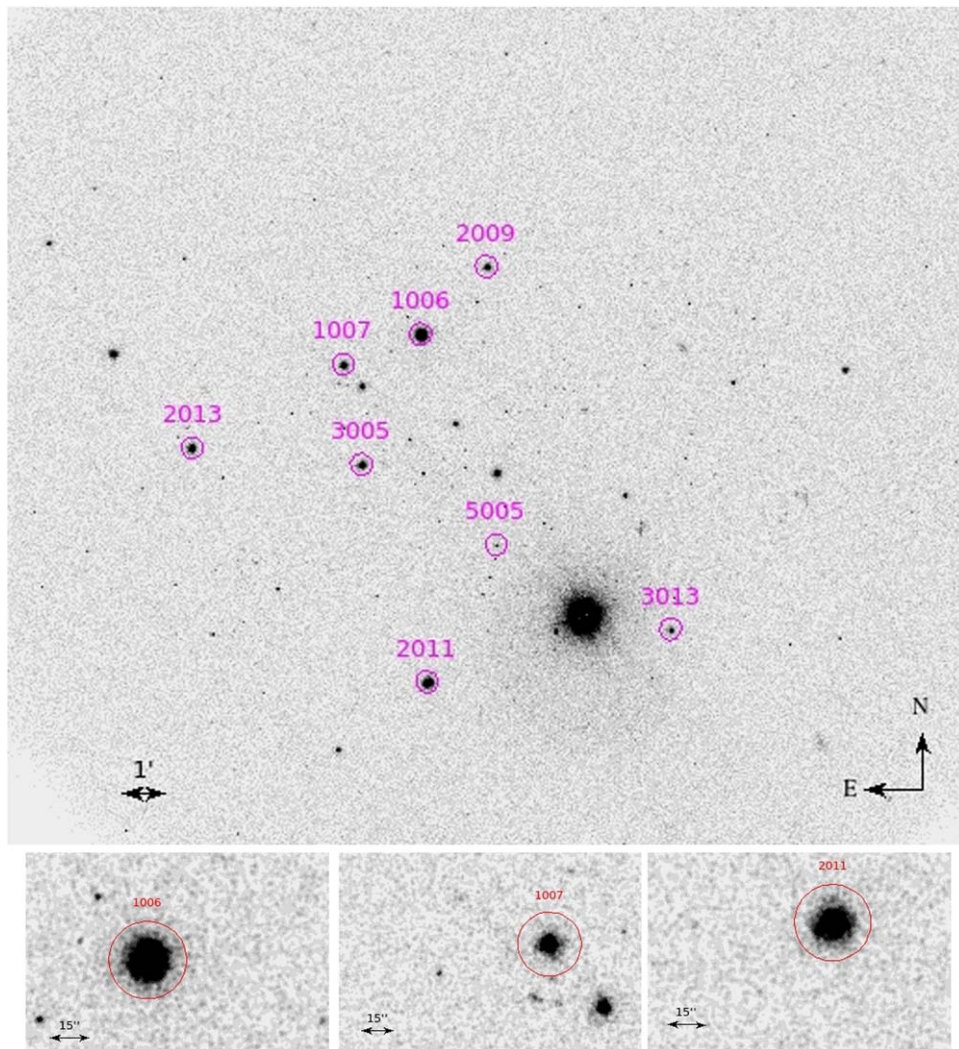


**Figure 1.** UVIT image of M67 obtained in the F148W filter. A few stars are marked in the image and stamp size images of the three stars studied here are shown below.

masses  $< 0.4 M_{\odot}$ , are formed from stars that never ignited helium in their cores. As single-star evolution takes more time than the age of the universe to form these WDs, formation of low-mass WDs require evolution in close binaries (Brown et al. 2010). Hence detection and characterization of the hot companion to WOCS1007 is extremely important to throw light on the formation pathways of both the BSS as well as the low-mass WD.

The Ultra-Violet Imaging Telescope (UVIT) on board the Indian space observatory, *ASTROSAT*, has been producing far-UV (FUV) and near-UV (NUV) images of superior resolution of  $\sim 1''.5$ , which is better than the *Galaxy Evolution Explorer (GALEX)* mission with its resolution of  $> 4''$  in the same wavelength bands. Here we present analyses and results for three BSSs (WOCS1006, 1007, and 2011) in M67 observed in three FUV filters of UVIT. We combine the UVIT magnitudes with other estimations in the UV, optical, and near-IR from space as well as ground observations to create a multi-wavelength spectral energy distribution (SED). We present the details of the data and observation in Section 2, SED fits in Section 3, and discussion in Section 4.

## 2. Observations and Data

M67 was observed in the F148W, F154W, and F169M filters, all observed on the same day. We were unable to get the NUV

data due to payload related issues and the visible filter data is useful only for drift correction. UVIT data were corrected for distortion, flat fielding, and spacecraft drift using the CCDLAB (Postma & Leahy 2017). Figure 1 shows the image in the F148W filter. Details of UVIT, in-orbit performance, and calibration are described in Subramaniam et al. (2016b) and Tandon et al. (2017a, 2017b).

Point-spread function photometry was performed using standard IRAF routines to obtain the magnitudes in all the filters, which are also corrected for aperture and saturation (Tandon et al. 2017b). The limiting magnitude in all UVIT filters is  $\sim 22$  mag, with a maximum error of 0.2 mag. The UVIT observation details are listed in Table 1, along with already available observations, which are used in this study. As two are binaries, which can show photometric variability on timescales comparable to or shorter/longer than the exposure or cadence times, the date of observations are provided in Table 1.

## 3. Spectral Energy Distribution

The aim of this study is to check for the presence of hot companions to BSSs using the FUV flux detected by UVIT. Here we restrict our study to three of the confirmed 14 BSSs by Geller et al. (2015). We study the potential candidate WOCS1007 for which a WD companion is expected based on its orbital solutions,

**Table 1**  
Details of All Observations Used in This Study

| Date of Observation | Filter     | Exposure Time (s) | $\lambda_{\text{eff}}$ ( $\text{\AA}$ ) | $\Delta\lambda$ ( $\text{\AA}$ ) | $m_{zp}$ |
|---------------------|------------|-------------------|---|----------------------------------|----------|
| 2017 Apr 23         | UVIT F148W | 2290              | 1481                                    | 500                              | 18.016   |
| 2017 Apr 23         | UVIT F154W | 2428              | 1541                                    | 380                              | 17.778   |
| 2017 Apr 23         | UVIT F169M | 2428              | 1608                                    | 290                              | 17.455   |
| 2006 Jan 21         | GALEX FUV  | 5555.2            | 1542                                    | 255                              | 18.82    |
| 2006 Jan 21         | GALEX NUV  | 5555.2            | 2274                                    | 729                              | 20.08    |
| 1986 Mar 18         | IUE NUV    | 1200              | 1900–3200                               | 7 <sup>a</sup>                   |          |
| 1986 Mar 19         | IUE NUV    | 1800              | 1900–3200                               | 7 <sup>a</sup>                   |          |
| 1986 Mar 20         | IUE NUV    | 2100              | 1900–3200                               | 7 <sup>a</sup>                   |          |
| 1986 Mar 18         | IUE FUV    | 4500              | 1150–1950                               | 7 <sup>a</sup>                   |          |
| 1986 Mar 19         | IUE FUV    | 7267              | 1150–1950                               | 7 <sup>a</sup>                   |          |
| 1987 Dec 15         | IUE FUV    | 3600              | 1150–1950                               | 7 <sup>a</sup>                   |          |
| 1990 Feb 15–18      | KPNO U     | 900               | 3630                                    | 592                              |          |
| 1990 Feb 15–18      | KPNO B     | 480               | 4358                                    | 1004                             |          |
| 1990 Feb 15–18      | KPNO V     | 240               | 5366                                    | 939                              |          |
| 1990 Feb 15–18      | KPNO I     | 240               | 8100                                    | 1825                             |          |
|                     | GAIA2 Gbp  |                   | 5050                                    | 2347                             | 25.3806  |
|                     | GAIA2 G    |                   | 6230                                    | 4183                             | 25.7934  |
|                     | GAIA2 Grp  |                   | 7730                                    | 2756                             | 25.1161  |
| 1997 Nov 16         | 2MASS J    | 403               | 12350                                   | 1624                             | 21.039   |
| 1997 Nov 16         | 2MASS H    | 403               | 16620                                   | 2509                             | 20.696   |
| 1997 Nov 16         | 2MASS K    | 403               | 21590                                   | 2618                             | 20.05    |
| 2010 Apr 29         | WISE W1    |                   | 33526                                   | 6626                             | 20.5     |
| 2010 Apr 29         | WISE W2    |                   | 46028                                   | 10422                            | 19.5     |
| 2010 Apr 28         | WISE W3    |                   | 115608                                  | 55055                            | 18.0     |

**Notes.** The first column provides the date of observation (based on the availability). The filter details and exposure times are given in the second and third columns. The fourth and fifth columns list the effective wavelength and bandwidth of the filter. The zero-point magnitudes are listed in column 6.

<sup>a</sup> Spectral Resolution

**Table 2**

The Observed Photometric Flux and Their Respective Errors of the Three BSSs Detected in the Three FUV Filters of UVIT Are Listed along with Other Filters From UV to IR

| WOCS ID<br>Filter           | 1006  |  | 1007  |  | 2011  |  |
|-----------------------------|---|--|---|--|---|--|
|                             | Observed Flux<br>( $\text{erg s}^{-1} \text{cm}^{-2} \text{\AA}^{-1}$ ) | Observed Error<br>( $\text{erg s}^{-1} \text{cm}^{-2} \text{\AA}^{-1}$ ) | Observed Flux<br>( $\text{erg s}^{-1} \text{cm}^{-2} \text{\AA}^{-1}$ ) | Observed Error<br>( $\text{erg s}^{-1} \text{cm}^{-2} \text{\AA}^{-1}$ ) | Observed Flux<br>( $\text{erg s}^{-1} \text{cm}^{-2} \text{\AA}^{-1}$ ) | Observed Error<br>( $\text{erg s}^{-1} \text{cm}^{-2} \text{\AA}^{-1}$ ) |
| <i>Astrosat</i> /UVIT.F148W | 4.97E–14  | 1.83E–16   | 7.61E–15  | 1.26E–16   | 2.29E–14  | 3.59E–16   |
| <i>Astrosat</i> /UVIT.F154W | 5.32E–14  | 7.84E–16   | 8.17E–15  | 1.20E–16   | 2.53E–14  | 2.57E–16   |
| GALEX/GALEX.FUV             | 5.53E–14  | 1.19E–16   | 6.13E–15  | 2.58E–16   | 2.14E–14  | 2.86E–16   |
| <i>Astrosat</i> /UVIT.F169M | 5.65E–14  | 8.85E–16   | 9.31E–15  | 1.63E–16   | 2.81E–14  | 1.81E–16   |
| IUE/IUE.1675–1725           | 1.01E–13  | 5.34E–15   | 2.08E–14  | 7.67E–15   | 4.73E–14  | 2.91E–15   |
| IUE/IUE.2150–2200           | 1.02E–13  | 2.78E–14   | 5.61E–14  | 2.85E–14   | 7.16E–14  | 1.89E–14   |
| GALEX/GALEX.NUV             | 9.50E–14  | 2.87E–16   | 5.97E–14  | 3.27E–16   | 7.07E–14  | 2.37E–16   |
| IUE/IUE.2395–2445           | 7.87E–14  | 9.57E–15   | 4.14E–14  | 1.04E–14   | 5.33E–14  | 6.54E–15   |
| IUE/IUE.2900–3000           | 1.07E–13  | 4.31E–15   | 8.42E–14  | 5.85E–15   | 7.71E–14  | 3.15E–15   |
| KPNO/Mosaic.B               | 2.27E–13  | 6.77E–14   | 2.15E–13  | 1.20E–13   | 1.70E–13  | 4.96E–14   |
| GAIA/GAIA2.Gbp              | 1.69E–13  | 5.05E–14   | 1.64E–13  | 9.17E–14   | 1.25E–13  | 3.64E–14   |
| KPNO/Mosaic.V               | 1.52E–13  | 4.53E–14   | 1.59E–13  | 8.91E–14   | 1.17E–13  | 3.39E–14   |
| GAIA/GAIA2.G                | 1.08E–13  | 3.22E–14   | 1.13E–13  | 6.33E–14   | 8.02E–14  | 2.33E–14   |
| GAIA/GAIA2.Grp              | 6.01E–14  | 1.79E–14   | 7.14E–14  | 4.00E–14   | 4.54E–14  | 1.32E–14   |
| KPNO/Mosaic.I               | 4.93E–14  | 1.47E–14   | 6.12E–14  | 3.43E–14   | 3.95E–14  | 1.15E–14   |
| 2MASS/2MASS.J               | 1.57E–14  | 2.61E–16   | 2.10E–14  | 3.50E–16   | 1.22E–14  | 1.92E–16   |
| 2MASS/2MASS.H               | 5.65E–15  | 9.38E–17   | 8.29E–15  | 1.53E–16   | 4.38E–15  | 7.26E–17   |
| 2MASS/2MASS.Ks              | 2.24E–15  | 3.72E–17   | 3.34E–15  | 4.93E–17   | 1.72E–15  | 2.53E–17   |
| WISE/WISE.W1                | 4.69E–16  | 9.50E–18   | 6.75E–16  | 1.43E–17   | 3.39E–16  | 6.56E–18   |
| WISE/WISE.W2                | 1.32E–16  | 2.55E–18   | 1.95E–16  | 3.59E–18   | 9.76E–17  | 1.88E–18   |
| WISE/WISE.W3                | 3.50E–18  | 3.21E–19   | 5.20E–18  | 3.50E–19   |   |  |

**Note.** GALEX—FUV and NUV flux are taken from the GR6/GR7 data release and corrected for saturation, the optical flux from Montgomery et al. (1993), and IUE, 2MASS, WISE, and GAIA are taken from their respective source catalogue through Virtual Observatory photometry.

**Table 3**  
Fundamental Parameters of the BSS and WD Companion

| WOCS ID  | S No. | $T_{\text{eff}}$ (K) | $\log g$ | $L/L_{\odot}$    | $R/R_{\odot}$    | $\chi_{\text{red}}^2$     |
|----------|-------|----------------------|----------|------------------|------------------|---------------------------|
| 1006     | 1066  | $8750 \pm 125$       | 3.0      | $26.75 \pm 0.72$ | $2.31 \pm 0.03$  | 40.2 (11.2 <sup>†</sup> ) |
|          |       | $8750 \pm 125$       | 3.5      | $26.45 \pm 0.90$ | $2.26 \pm 0.03$  | 2.2 <sup>§</sup>          |
| 2011     | 968   | $8500 \pm 125$       | 4.0      | $19.76 \pm 0.78$ | $2.10 \pm 0.03$  | 52.2(21.5 <sup>†</sup> )  |
|          |       | $8750 \pm 125$       | 3.5      | $19.79 \pm 0.54$ | $1.96 \pm 0.03$  | 0.9 <sup>§</sup>          |
| 1007-BSS | 1284  | $7750 \pm 125$       | 3.0      | $26.14 \pm 0.74$ | $2.97 \pm 0.04$  | 44.1(31.7 <sup>†</sup> )  |
|          |       | $7500 \pm 125$       | 3.5      | $24.57 \pm 1.01$ | $2.94 \pm 0.04$  | 2.7 <sup>§</sup>          |
| 1007-WD  |       | $13250 \pm 125$      | 6.5      | $0.26 \pm 0.05$  | $0.097 \pm 0.01$ | 3.3                       |
|          |       | $13250 \pm 125$      | 7.75     | $0.24 \pm 0.05$  | $0.094 \pm 0.01$ | 2.5                       |
|          |       | $13750 \pm 125$      | 9.0      | $0.29 \pm 0.06$  | $0.095 \pm 0.01$ | 2.4                       |

**Note.** The first and second columns list the WOCS and Sanders numbers, Third, fourth, fifth, and sixth columns list the  $T_{\text{eff}}$ ,  $\log g$ , luminosity, and radius estimated for BSS (WOCS1006 and WOCS2011), and BSS and WD companion (WOCS1007), respectively.  $\chi_{\text{red}}^2$  for the single fit is listed in the seventh column. In the case of WOCS1007, the first row lists the  $\chi_{\text{red}}^2$  for the step 1 fit, second row for the step 2 fit, and the last three rows for the composite fit.

along with WOCS1006 and WOCS2011, as these have *IUE* spectra. WOCS1006 and WOCS1007 are known to be single-lined spectroscopic binaries and Mathys (1991) have identified WOCS2011 as an Am star and Geller et al. (2015), through their radial velocity membership study, have classified this star as a single member. WOCS1007 is a  $\delta$  Scuti variable that shows pulsations in 26 frequencies with a maximum amplitude of 3 mmag at 230  $\mu\text{Hz}$  (Bruntt et al. 2007). Sindhu et al. (2018) inspected the *IUE* spectra and found the 2800 Å Mg II spectral line to be in absorption in all three stars, suggesting no/insignificant chromospheric activity in these stars. We check whether the detected FUV fluxes are in agreement with those expected for the BSSs, which in turn requires an accurate estimation of the properties of BSSs. Sindhu et al. (2018) used SED analysis to estimate their properties, which are listed in their Table 4.

The UVIT fluxes (F148W, F154W, and F169M) are combined with fluxes from *GALEX* (Martin et al. 2005; FUV and NUV), *IUE* (Boggess et al. 1978; 1250, 1450, 1675, 2150, 2395, 2900 Å—photometry from spectra), optical (Montgomery et al. 1993; *UBVRI*), *Gaia* (Gaia Collaboration et al. 2018;  $G_{\text{bp}}$ ,  $G$ ,  $G_{\text{rp}}$ ), Two Micron All Sky Survey (2MASS, Cohen et al. 2003; JHKs), and Wide-field Infrared Survey Explorer (*WISE*, Wright et al. 2010; W1, W2 and W3). Multiwavelength SEDs with photometric flux from UV to IR listed in Table 2, spanning a wavelength range of 0.14–11.5  $\mu\text{m}$ , covered by a maximum of 23 data points, are constructed after correcting for extinction in the respective bands (Fitzpatrick 1999). We adopted  $E(B-V) = 0.041 \pm 0.004$  mag (Taylor 2007), distance modulus  $V-M_v = 9.6 \pm 0.04$  mag, and solar metallicity. We used the virtual-observatory SED analyzer (VOSA) to fit the SEDs and the details can be found in Sindhu et al. (2018).

The SED fits for the three stars are performed using the following three steps.

*Step 1.* We first performed a single spectral fit to the SEDs using the Kurucz models (Castelli et al. 1997 and updates) for the entire wavelength region, using the  $T_{\text{eff}}$  and  $\log g$  as found by Sindhu et al. (2018). The fluxes predicted by the model spectrum for the selected temperature and  $\log g$  for all the filters were estimated, which were then scaled to match the observed fluxes.  $\chi_{\text{red}}^2$  values estimated for these single spectral fits are tabulated in column 7 of the first row of Table 3. We estimated the  $\chi_{\text{red}}^2$  <sup>†</sup> value<sup>14</sup> for the same fit to compare with step 2. This value is shown in the parentheses (first row).

*Step 2.* As the  $\chi_{\text{red}}^2$  values are large, we repeat step 1 by fitting the SEDs excluding the photometric bandpass shorter than 1800 Å to ignore any unusual UV flux and to refine the fit in the NUV–optical–IR region. The best-fit  $\chi_{\text{red}}^2$  <sup>§</sup> values<sup>15</sup> are tabulated in column 7 and the second row of Table 3. The step 2 fit is used to check for a mismatch between the observed and the model SED in the shorter wavelengths and detect excess/deficient flux in the UV with respect to the expected BSS UV flux.

*Step 3.* For both of the above fits, we estimated error weighted residual (EWR) flux using the equation

$$\text{EWR} = (\text{Flux}_{\text{Obs}} - \text{Flux}_{\text{Model}}) / \text{Err}_{\text{Obs}}. \quad (1)$$

The SEDs of the BSSs are shown in Figure 2, and we discuss them below.

### 3.1. WOCS1006

Step 1 is performed using 23 photometric points with two fitting parameters and the number of degrees of freedom (Ndof) = 21. The SED fit shows a large  $\chi_{\text{red}}^2$  value of 40.2 and a  $\chi_{\text{red}}^2$  <sup>†</sup> value of 11.2 (Figure 2(a); EWR in the bottom panel). We repeat the fit using step 2 (Figure 2(b)) to obtain a better  $\chi_{\text{red}}^2$  <sup>§</sup> value of 2.2. Step 2 improves the flux residual in the optical and IR bands, with a slight excess in the UV region, as seen in one UVIT filter and *GALEX* FUV (Figure 2(b), bottom panel). As excess UV flux is not detected in the other two UVIT filters, we consider this star to be either a single BSS or a binary with a photometrically undetectable companion.

### 3.2. WOCS2011

Step 1 is performed using 22 photometric points with two fitting parameters (Ndof=20). The SED fit shows a large  $\chi_{\text{red}}^2$  (52.2) and  $\chi_{\text{red}}^2$  <sup>†</sup> values (21.5). The observed flux is more than the synthetic flux in the UV region, and vice versa in the longer wavelengths (Figure 2(c)). We repeat the fit using step 2 (Figure 2(d)) and the best fit shows a lower  $\chi_{\text{red}}^2$  <sup>§</sup> value of 0.9, suggesting a good fit and an improvement in the residual in the longer wavelengths. On the other hand, a deficiency in the FUV flux is found, as seen in the EWR plot (Figure 2(d)). Step 2 also increases the  $T_{\text{eff}}$  from 8500 to 8750 K. Nicolet & Cramer (1983) studied Am stars in the UV wavelength and observed significant deficiency of flux below 1800 Å, which is in

<sup>14</sup>  $\chi_{\text{red}}^2$  values calculated by ignoring filters with  $\lambda_{\text{eff}} < 1800\text{Å}$  for a full single spectral fit (FUV to IR) are represented by “†.”

<sup>15</sup>  $\chi_{\text{red}}^2$  values obtained after a single spectral fit (NUV to IR) excluding filters with  $\lambda_{\text{eff}} < 1800\text{Å}$  are represented by “§.”

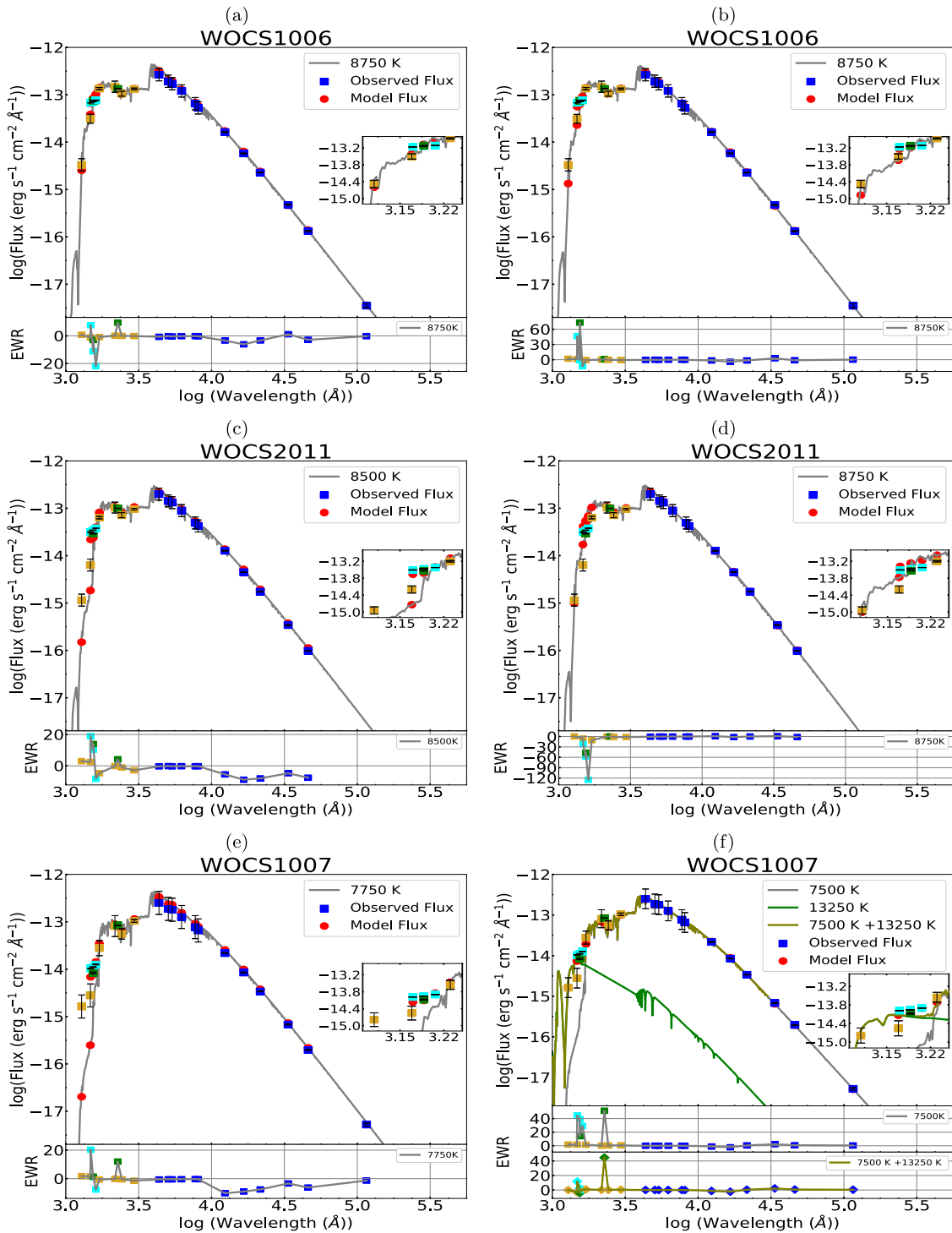


**Figure 2.** SEDs of three BSSs with the close-up of the UV region in the insets. Left panels show the step 1 SED fits. Right panels show the step 2 SEDs for WOCS1006 and WOCS2011, and double fit for WOCS1007. The scaled and best-fitting Kurucz spectrum (gray), Koester WD spectrum (green), and composite spectrum (olive) are shown along with corresponding  $T_{\text{eff}}$ . The observed photometric flux corrected for extinction are shown with blue (from optical to IR), cyan (UVIT), green (*GALEX*), and gold squares (*IUE*), and the corresponding composite synthetic flux as red dots. The EWR plots are in the bottom panels.

agreement with this study. Thus, WOCS2011 is likely to be a BSS with a deficient flux in FUV.

### 3.3. WOCS1007

Step 1 is performed using 23 photometric points with two fitting parameters ( $N_{\text{dof}} = 21$ ). In the SED, the presence of an excess UV flux can be inferred from the observed data points extending significantly to the FUV region, when compared to

the continuum shown in gray (Figure 2(e)). The SED fit shows a large  $\chi_{\text{red}}^2$  (44.1) and  $\chi_{\text{red}}^2 \dagger$  (31.7) values. We repeat the fit using step 2, which brings down the  $\chi_{\text{red}}^2 \S$  (2.7). This fit results in the detection of a statistically significant excess flux in all three UVIT FUV filters and the *GALEX* FUV filter, (Figure 2(f), middle panel). As the residual (EWR) is weighted by error, the *IUE* data points do not show statistically significant excess due to a large error, even though we detect

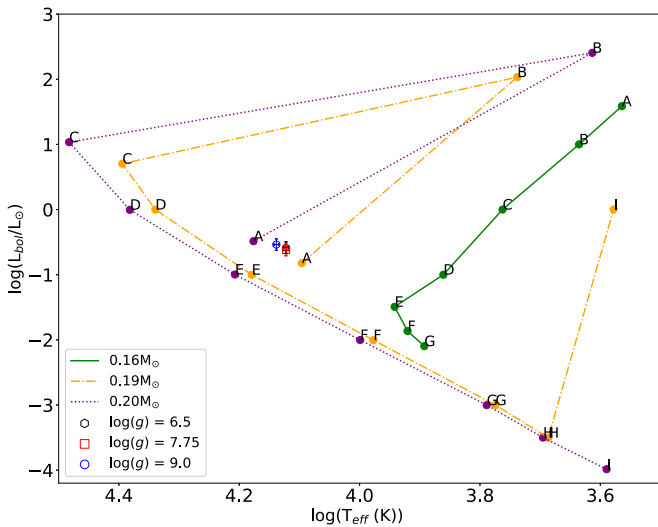


**Figure 3.** H–R diagram of He WD model taken from Table 3 of Panei et al. (2007) is plotted for  $0.16M_{\odot}$ ,  $0.19M_{\odot}$ , and  $0.20M_{\odot}$ . The characteristics of each labeled point are described in their Table 3. The end of binary evolution (which is the starting point of WD evolution) is denoted by point A in the figure. The estimated parameters of WOCS1007 are shown in the plot for three  $\log g$  values 6.5, 7.75, and 9

$\sim 50\%$  more flux than those expected for the BSS in UVIT, *GALEX*, and *IUE* filters. The residual plot of WOCS1007 also shows that the companion is likely to be a subluminal object (in comparison to Figure 2 of Subramaniam et al. 2016a).

We used Koester spectral models (Tremblay & Bergeron 2009; Koester 2010) to fit the UV excess in the SED. In Kepler et al. (2015), most of the WDs are found to have  $\log g \sim 8$  (their Figures 4, 5, and 6). Therefore, we used three values of  $\log g$  (6.5, 7.75, and 9.0), though the broadband fluxes used in the SED are quite insensitive to the choice. As the fluxes of the hot component and BSS get added up, we created a composite SED in order to fit the full observed SED from UV to IR. The composite model SED is created by computing model fluxes for the BSS and WD, and adding the individually scaled fluxes. Though the parameters (radius and temperature) of the WD spectra are mainly varied for the  $\chi^2$  minimization, minor modifications of the BSS parameters were also done to obtain the overall good fit over the entire wavelength range. Adopting a range in extinction values from the literature does not change the obtained parameters by more than  $3\sigma$ .

We have used 21 data points for the double SED fit (Figure 2(f)) with three fitting parameters (Ndof = 18). F148W and *GALEX* NUV points were not used, as the  $\chi^2_{\text{red}}$  value increases due to small photometric errors, though the estimated parameters were not found to change significantly. The EWR plot (bottom panel) suggests almost zero residual, except for one *GALEX* NUV data point with large deviation due to a small error. The reduction of the  $\chi^2_{\text{red}}$  value (44.1–2.5) favors the double fit, with  $>95\%$  confidence.

We estimated the WD to have  $T_{\text{eff}} = 13,250\text{--}13,750$  K (depending on the  $\log g$ ),  $L/L_{\odot} = 0.24\text{--}0.28$ , and  $R/R_{\odot} = 0.094 \pm 0.01\text{--}0.097 \pm 0.01$  (assuming a 10% error in distance to M67, as the uncertainty of the distance with different distance modulus from various surveys). In Figure 3, we have shown the evolutionary tracks for low-mass helium WD models from Panei et al. (2007) for  $0.16M_{\odot}$ ,  $0.19M_{\odot}$ , and  $0.20M_{\odot}$ . The evolution of the WD begins after the mass-loss phase at the point A labeled (which is also the end of binary

evolution) in Figure 3 for all three WD models. Further details of each point on the evolutionary track can be referred from their Table 3. We have shown the star WOCS1007 with all three  $\log g$  values in the same figure. When we compare our estimated parameters to the WD model parameters, we find the closest match for low-mass helium WD models for a  $0.19M_{\odot}$  or a  $0.20M_{\odot}$  He WD. This suggests that the hot companion to WOCS1007 is likely to be a low-mass WD.

#### 4. Discussion

We have shown the observed and model estimated flux for *IUE*, UVIT, and *GALEX* along with the observed extinction corrected spectra of *IUE* in Figure 4. The flux from the UVIT filters are consistent with the observed *IUE* spectra. The rising trend in the *IUE* spectrum below  $1250\text{ \AA}$  is due to the geocoronal Ly $\alpha$  line, whereas UVIT filters do not detect it. Figure 4 confirms the presence of UV excess in the case of WOCS1007, as traced by the continuum of the *IUE* FUV spectrum. The *IUE* spectrum and the fitted spectral model for the hot component agree well, confirming the detection of the WD companion. In the case of WOCS2011, the *IUE* FUV spectrum also shows the presence of a deficiency in the FUV flux.

WOCS1007 is a short-period eccentric binary (Latham et al. 1992) and a fast rotator ( $v \sin i$  of  $80\text{ km s}^{-1}$  by Milone et al. 1991;  $79.45\text{ km s}^{-1}$  by Bertelli Motta et al. 2018). Our estimate of the secondary mass from the Panei et al. (2007) models suggests a  $\sim 0.19\text{--}0.20M_{\odot}$  WD. This is in agreement with the kinematic estimate of the secondary mass ( $M_2 \sin i = 0.19\text{--}0.21M_{\odot}$ ) by Latham et al. (1992) for a primary ( $M_1$ ) mass of  $2.0\text{--}2.2M_{\odot}$ . This makes the secondary companion belong to the class of low-mass WDs, which are formed only in close binaries, as single-star evolution prohibits the formation of WDs with mass less than  $0.4M_{\odot}$  within the Hubble time (Brown et al. 2010; Istrate et al. 2016). The accepted mechanism for the formation of low-mass He-core WDs is either through unstable mass loss via common-envelope episodes or stable mass loss via Roche-Lobe overflow in close binaries (Istrate et al. 2016; Calcaferro et al. 2018).

The WD companion of WOCS1007 is consistent with He WD models, with a luminosity of  $0.1\text{--}0.15L_{\odot}$  which is within  $3\sigma$  from our estimated value. In Figure 3, the WD lies close to the points labeled A and E of the  $0.19M_{\odot}$  and  $0.20M_{\odot}$  models. If we consider that the WD is at the point A, then the WD is recently formed and is still evolving toward a typical WD. It also demands the MT to have stopped very recently, as supported by the large rotation of the BSS. On the other hand, if we consider that the WD is at the evolutionary point E, then the WD is formed about  $\sim 190$  Myr ago for a  $0.19M_{\odot}$  or  $\sim 160$  Myr for a  $0.20M_{\odot}$ .

Lu et al. (2010) studied the formation of BSSs via MT in close binaries in M67. They followed the evolution of a close binary ( $\sim 1.4$  days with circular orbit) of  $1.4M_{\odot} + 0.9M_{\odot}$  and compared the evolutionary behavior of case A and B MT cases. The end product of the close binary pair was found to be a  $2.04M_{\odot}$  BSS with a  $0.26M_{\odot}$  WD companion, which is very similar to the WOCS1007 system. Presently, the BSS is estimated to have a mass of  $2.0\text{--}2.2M_{\odot}$ , which demands that it has gained at least  $0.7\text{--}0.9M_{\odot}$  (assuming its progenitor to be a  $1.3M_{\odot}$  star and more, if it is less massive). The progenitor of the WD, expected to be  $\sim 1.35M_{\odot}$ , would have therefore transferred at least  $0.7\text{--}0.9M_{\odot}$  to the secondary during the MT, which is  $\geq 50\%$  to its original mass. This demands an efficient MT and hence a case A/B MT may be preferred to other types of MT, such as, a wind accretion model (Perets 2015). A detailed

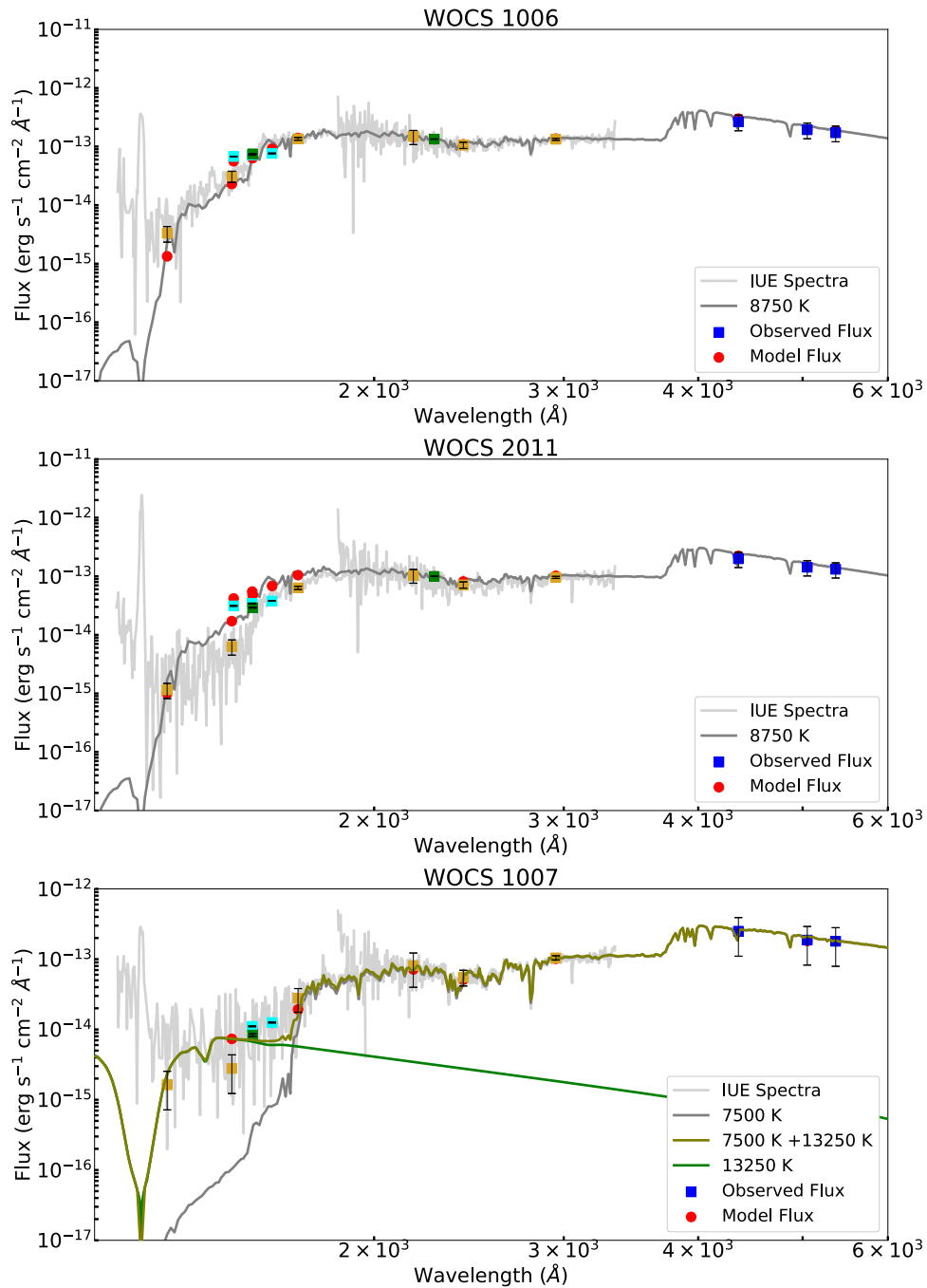


**Figure 4.** SEDs of three BSSs (WOCS1006, WOCS2011, and WOCS1007) along with *IUE* spectra corrected for extinction. The colors codes are similar to Figure 2.

simulation of WOCS1007 is necessary to derive the details of the progenitors as well as the mode of MT which created the present configuration.

WOCS2011 is known to be an Am star (Mathys 1991) and is a slow rotator ( $\sim$ a few  $\text{km s}^{-1}$  by Milone et al. 1991), and could have slowed down due to magnetic braking. We find the star to have deficient flux in FUV, which is typical for the Am stars. On the other hand, it is likely to have no/less chromospheric activity as indicated by the 2800 Å Mg II absorption line.

WOCS1006 is one of the fast rotating BSSs with a  $v \sin i$  of  $100 \text{ km s}^{-1}$  (Milone et al. 1991). WOCS1006 does not have a detectable WD companion, though it is known to be a single-lined spectroscopic binary. It is possible that this is also a post-MT object, as suggested by its fast rotation, where the WD

companion has cooled enough by now and is no longer detectable, and there is no magnetic activity for the BSS to spin down. It should be noted that there is a limited window to actually be able to detect these WD companions photometrically before they cool down and become too faint relative to the BSSs. It is thus essential to monitor their radial velocities to detect companions and constrain their masses, wherever possible.

This study presents the first detection of a low-mass He WD as a companion to a BSS. Previous detections of such WDs in binary systems are mostly in double degenerate systems, where the companion is either a neutron star or a normal WD (Liebert et al. 2004; Vennes et al. 2011, and references therein). It is also the first time such a low-mass WD is detected in the well-

studied M67 cluster. This discovery will therefore help identify/constrain the formation pathways of not only the low-mass He-WDs but also the BSSs.

**Summary.** We report the first detection of a WD companion to one of the BSSs (WOCS1007) in M67, using FUV images from the UVIT on *ASTROSAT*. The WD companion is found to have a  $T_{\text{eff}} \sim 13,250\text{--}13,750$  K and a radius of  $0.09 R_{\odot}$ , comparable to a He WD of  $0.18 M_{\odot}$ , confirming it to be a low-mass WD. As single-star evolution cannot produce a low-mass WD within the Hubble time, formation through MT in close binaries is necessary. Thus, we suggest that WOCS1007 is formed as a result of a MT in a close binary, possibly through a case A or case B binary evolution. We also detect a deficiency in the FUV flux for WOCS2011, which is an Am star.

The *UVIT* project is a result of the collaboration between IIA, Bengaluru, IUCAA, Pune, TIFR, Mumbai, several centers of ISRO, and CSA. This publication makes use of VOSA, developed under the Spanish Virtual Observatory project supported from the Spanish MICINN through grant AyA2008-02156. S.N. acknowledges support from CSIR for the grant 09/890(0005)/17 EMR-I. We thank the anonymous referee for the useful comments.

### ORCID iDs

N. Sindhu  <https://orcid.org/0000-0001-6006-1727>  
 Vikrant V. Jadhav  <https://orcid.org/0000-0002-8672-3300>  
 Sourav Chatterjee  <https://orcid.org/0000-0002-3680-2684>  
 Aaron M. Geller  <https://orcid.org/0000-0002-3881-9332>  
 Thomas H. Puzia  <https://orcid.org/0000-0003-0350-7061>  
 Michael Shara  <https://orcid.org/0000-0003-0155-2539>

### References

- Bertelli Motta, C., Pasquali, A., Caffau, E., & Grebel, E. K. 2018, *MNRAS*, **480**, 4314  
 Boggess, A., Carr, F. A., Evans, D. C., et al. 1978, *Natur*, **275**, 372  
 Brown, W. R., Kilic, M., Allende Prieto, C., & Kenyon, S. J. 2010, *ApJ*, **723**, 1072  
 Bruntt, H., Stello, D., Suárez, J. C., et al. 2007, *MNRAS*, **378**, 1371  
 Calcaferro, L. M., Córscico, A. H., Althaus, L. G., Romero, A. D., & Kepler, S. O. 2018, *A&A*, **620**, A196  
 Castelli, F., Gratton, R. G., & Kurucz, R. L. 1997, *A&A*, **318**, 841  
 Cohen, M., Wheaton, W. A., & Megeath, S. T. 2003, *AJ*, **126**, 1090  
 Fitzpatrick, E. L. 1999, *PASP*, **111**, 63  
 Gaia Collaboration, Brown, A. G. A., Vallenari, A., et al. 2018, *A&A*, **616**, A1  
 Geller, A. M., Hurley, J. R., & Mathieu, R. D. 2013, *AJ*, **145**, 8  
 Geller, A. M., Latham, D. W., & Mathieu, R. D. 2015, *AJ*, **150**, 97  
 Gosnell, N. M., Mathieu, R. D., Geller, A. M., et al. 2015, *ApJ*, **814**, 163  
 Hills, J. G., & Day, C. A. 1976, *ApJL*, **17**, 87  
 Istrate, A. G., Marchant, P., Tauris, T. M., et al. 2016, *A&A*, **595**, A35  
 Kepler, S. O., Pelisoli, I., Koester, D., et al. 2015, *MNRAS*, **446**, 4078  
 Knigge, C., Dieball, A., Maíz Apellániz, J., et al. 2008, *ApJ*, **683**, 1006  
 Knigge, C., Leigh, N., & Sills, A. 2009, *Natur*, **457**, 288  
 Koester, D. 2010, *MmSAI*, **81**, 921  
 Landsman, W., Bohlin, R. C., Neff, S. G., et al. 1998, *AJ*, **116**, 789  
 Latham, D. W., Mathieu, R. D., Milone, A. A. E., & Davis, R. J. 1992, in ASP Conf. Ser. 32, IAU Coll. 135: Complementary Approaches to Double and Multiple Star Research, ed. H. A. McAlister & W. I. Hartkopf (San Francisco, CA: ASP), 152  
 Leigh, N., & Sills, A. 2011, *MNRAS*, **410**, 2370  
 Liebert, J., Bergeron, P., Eisenstein, D., et al. 2004, *ApJL*, **606**, L147  
 Lu, P., Deng, L. C., & Zhang, X. B. 2010, *MNRAS*, **409**, 1013  
 Martin, D. C., Fanson, J., Schiminovich, D., et al. 2005, *ApJL*, **619**, L1  
 Mathieu, R. D., & Geller, A. M. 2009, *Natur*, **462**, 1032  
 Mathys, G. 1991, *A&A*, **245**, 467  
 McCrea, W. H. 1964, *MNRAS*, **128**, 147  
 Milone, A. A. E., & Latham, D. W. 1992, *International Astronomical Union*, **151**, 475  
 Milone, A. A. E., Latham, D. W., Kurucz, R. L., & Morse, J. A. 1991, in ASP Conf. Ser. 13, The Formation and Evolution of Star Clusters, ed. K. Janes (San Francisco, CA: ASP), 424  
 Montgomery, K. A., Marschall, L. A., & Janes, K. A. 1993, *AJ*, **106**, 181  
 Naoz, S., & Fabrycky, D. C. 2014, *ApJ*, **793**, 137  
 Nicolet, B., & Cramer, N. 1983, *A&A*, **117**, 248  
 Panci, J. A., Althaus, L. G., Chen, X., & Han, Z. 2007, *MNRAS*, **382**, 779  
 Perets, H. B. 2015, *ASSL*, **413**, 251  
 Perets, H. B., & Fabrycky, D. C. 2009, *ApJ*, **697**, 1048  
 Postma, J. E., & Leahy, D. 2017, *PASP*, **129**, 115002  
 Sahu, S., Subramaniam, A., Simunovic, M., et al. 2019, *ApJ*, **876**, 34  
 Shetrone, M. D., & Sandquist, E. L. 2000, *AJ*, **120**, 1913  
 Sindhu, N., Subramaniam, A., & Radha, C. A. 2018, *MNRAS*, **481**, 226  
 Subramaniam, A., Sindhu, N., Tandon, S. N., et al. 2016a, *ApJL*, **833**, L27  
 Subramaniam, A., Tandon, S. N., Hutchings, J., et al. 2016b, *Proc. SPIE*, **9905**, 99051F  
 Tandon, S. N., Hutchings, J. B., Ghosh, S. K., et al. 2017a, *JApA*, **38**, 28  
 Tandon, S. N., Subramaniam, A., Girish, V., et al. 2017b, *AJ*, **154**, 128  
 Taylor, B. J. 2007, *AJ*, **133**, 370  
 Tian, B., Deng, L., Han, Z., & Zhang, X. B. 2006, *A&A*, **455**, 247  
 Tremblay, P.-E., & Bergeron, P. 2009, *ApJ*, **696**, 1755  
 Vennes, S., Thorstensen, J. R., Kawka, A., et al. 2011, *ApJL*, **737**, L16  
 Wright, E. L., Eisenhardt, P. R. M., Mainzer, A. K., et al. 2010, *AJ*, **140**, 1868